Renewable Energy 186 (2022) 394–410

Contents lists available at ScienceDirect

Renewable Energy

journal homepage: www.elsevier.com/locate/renene

Modeling of soil-pile-structure interaction for dynamic response of standalone wind turbines

Shanghui Yang , Xiaowei Deng *, Jun Yang **

Department of Civil Engineering, The University of Hong Kong, Pokfulam, Hong Kong, China

ARTICLE INFO

Article history:
Received 4 August 2021
Received in revised form
19 November 2021
Accepted 14 December 2021
Available online 29 December 2021

Keywords:
Wind turbine
Foundation modeling
Soil-pile-structure interaction
Dynamic response
Distributed spring model
Apparent fixity model

ABSTRACT

The accurate prediction of the dynamic behavior of the offshore wind turbine plays a significant role in its safe and efficient operation, where special importance should be attached to the foundation modeling of soil-pile-structure interaction. The present study aims to compare the three foundation modeling approaches with special attention to their displacement, acceleration, and internal force response subject to the combined stochastic wind and wave loading. In addition, parametric studies have been conducted on the foundation modeling approaches with the focus on their sensitivity to the variation of the foundation stiffness, pile diameter, thickness, and pile embedded depth. Using the high-fidelity FE model of the soil-pile system as the benchmark, the apparent fixity model underestimates the foundation stiffness remarkably, while the distributed spring model can give a relatively accurate prediction of the foundation stiffness. Furthermore, the FE model of the soil-pile system is more sensitive to the soil densification and the pile embedded depth, while the apparent fixity model exhibits higher sensitivity to the pile diameter and thickness. Compared with the benchmark FE model, the study provides guidance for the applicability of the simplified foundation modeling approaches, the apparent fixity model and distributed spring model, to different foundation stiffness in engineering practice.

1. Introduction

The rapid economic development accompanied by the massive consumption of conventional fossil fuels brings about lots of serious environmental concerns, thus creating an urgent demand for clean and sustainable energy sources. Wind, as representative renewable energy, has experienced a rapid upsurge in the past decades, which demonstrates the potential to become a major contributor to global energy production in the future [1]. The early wind power industry mainly concentrated on the exploitation of onshore wind resources, and then it gradually shifts to the offshore counterpart with the further maturity of the construction technology [2]. Compared to the onshore wind power, the offshore one has several distinct advantages, including steadier and stronger wind speed, limited noise pollution, and large area available for the installation, which all lead to an increase in energy production. However, the special offshore environment also poses new challenges, like expensive installation, operation and maintenance costs, rough wind and wave conditions in the marine environment. To harness renewable energy in a more cost-effective manner, the foundation design is of great significance to the successful deployment of the wind turbine system in the offshore scenario.

As a common choice of foundation types, monopile gains its popularity for the offshore wind turbine installed in the shallow water owing to its simple structural form and convenient construction. However, on the other hand, the slenderness and flexibility of the structure make it more sensitive to the external dynamic excitation, especially exposed to complex aerodynamic and hydrodynamic loadings coming from wave and wind. During the whole lifetime of the offshore wind turbine, it is estimated the loading cycle of a wind turbine will reach 10^7 [3]. The adverse cyclic loadings may lead to excessive deformation of the structure, which not only compromises the power production but also affects the serviceability of the wind turbine; and for the worst situation, it may cause abrupt collapse. Therefore, it is of paramount importance to understand the dynamic behavior of the offshore wind turbine, which is fundamental to its safe and effective operation.

Several studies on the dynamic performance of the offshore wind turbine under combined wave and wind loadings have been conducted. In these studies, different kinds of assumptions were

* Corresponding author.
** Corresponding author.
E-mail addresses: xwdeng@hku.hk (X. Deng), junyang@hku.hk (J. Yang).

https://doi.org/10.1016/j.renene.2021.12.066
0960-1481/

made for the overall structure and loading conditions to simplify the analysis. For example, a standalone pile foundation was analyzed without considering the superstructure, where the distributed wave and wind loads were substituted with a resultant force and moment [4,5]. However, it is revealed that the soil-monopile-tower interaction affects the dynamic characteristics of the offshore wind turbine significantly and the serviceability criteria need to be considered separately for the tower top and seabed, which means that the accurate prediction of the structural response calls for the comprehensive analysis of the overall soil-pile-structure system [6,7]. On the other hand, some studies incorporate the effect of soil-pile interaction in the modeling of the OWT superstructures by the use of fixity end or linear and nonlinear springs [8–14]. Among these methods, the *p-y* curve method is commonly accepted for the soil-pile interaction simulation in research or engineering practice. which establishes the nonlinear relationship between the lateral displacement and loading by backcalculating from the field test [15]. Nevertheless, the applicability of the *p-y* curve method suffers from several limitations, especially to the situation of site-specific soil and numerous loading cycles [16]. Moreover, the substitute of the uncoupled springs ignores the continuum effect of the soil bed [17,18].

There are few studies on the dynamic behavior of the offshore wind turbine accounting for soil-pile-structure interaction, especially in terms of the sensitivity of the foundation modeling, e.g., apparent fixity model, distributed spring model, and FE model of the soil-pile system to the foundation stiffness [19,20]. Zuo et al. [21] studied the effects of operation condition and soil-structure interaction on the structural response of the offshore wind turbine, where the distributed spring model was adopted to characterize the soil-pile interaction. Ma et al. [22] investigated the influence of soil densification resulting from the long-term cyclic lateral loading on the turbine performance using the FE model of the soil-pile system, where the soil behavior was described by the Mhor-Coulomb constitutive model. Bush et al. [23] considered two alternative models for monopile foundation, apparent fixity model and distributed spring model, and compared the difference in the short-term response and extrapolated long-term response using FAST. Jung et al. [24] used the couple spring model at the mudline to simulate the soil-pile interaction and compared the difference of three foundation modelling approaches, i.e., boundary model, *p-y* curve-based spring model, and FEM-based spring model, in terms of time-domain characteristics of the structural response.

In this paper, three 3D finite element models based on the apparent fixity model, distributed spring model, and FE model of the soil-pile system are developed using ABAQUS to investigate the influence of the foundation modeling approaches on the dynamic performance of the offshore wind turbines when exposed to the combined wind and wave loadings. The structural responses are analyzed based on the time-domain and frequency-domain characteristics, with special attention to the tower top displacement and acceleration, and shear force at the mudline. Using the numerical models, a parametric analysis is performed to further discuss the sensitivity of the foundation characteristic parameters to the foundation stiffness, specifically involving the soil condition, pile diameter, pile thickness, and pile embedded length. Adopting the high-fidelity FE model of the soil-pile system as the benchmark, the study provides guidance on the applicability of two other simplified foundation modeling approaches, i.e., the apparent fixity model and the distributed spring model, to different foundation stiffness indexes proposed in this paper in practical engineering.

2. Numerical modeling

2.1. Integrated soil-pile-structure system

In this study, a three-bladed offshore 5-MW wind turbine situated in the East China Sea is selected as an example. The relevant structural parameters, provided by the manufacturer, are summarized in Table 1. Based on the reported data, the rotor-nacelle mass and rotor diameter are 334.8 tons and 126 m. The total length of the tower is 73 m, with the linear variation of outer diameter from 4.25 m to 6 m. The diameter and wall thickness of the pile are 6 m and 0.08 m, with the 35.5 m embedded depth below the seabed level. Young's modulus and Poisson ratio of the tower and monopile are taken as 210 GPa and 0.3, respectively. The soil profile parameters typical for offshore soil conditions in the East China Sea are considered for analysis, which are given in Table 2.

Three-dimensional finite element models based on three different foundation modeling approaches are developed using software ABAQUS, in which superstructures of all OWTs keep the same. The blades, rotor, nacelle, and hub are simplified as a point mass fixed at the top of the tower, which are modeled using shell element with a uniform cross section. Different element types are adopted for the three foundation models. For the apparent fixity foundation model, the monopile is modeled by beam element, of which the bottom is fixed at the depth of 3.5*D* below the mudline [11]. For the distributed spring model, monopile modeled by beam element is attached to distributed springs within the embedded part to consider soil-pile interaction. The substructure in the FE model of the soil-pile system is comprised of three parts, monopile, fill soil inside the pile, and outer soil outside the pile. The fill soil is assumed to fully plug the pile with the same length as the penetration depth [25], and the outer soil has a dimension of 10*D* in diameter and 1.6*L* in depth. The pile is modeled by shell element, while the soil domain is constructed using brick element, except surrounding with infinite element boundary to eliminate the artificial boundary effect on the dynamic response of the OWT [26]. Linear elastic behaviors are assumed for the monopile and tower, while the elastic-perfectly plastic Mhor-Coulomb constitutive model is used to characterize the complex material behavior of the

Table 1
Parameter of a representative 5-MW offshore wind turbine in the East China Sea.

Parameter	
Tower height (m)	73
Tower top diameter (m)	4.25
Tower bottom diameter (m)	6
Tower wall thickness (m)	0.04
Tower mass (kg)	170300
Young's modulus of tower material (GPa)	210
Top mass (kg)	334800
Monopile diameter (m)	6
Monopile wall thickness (m)	0.08
Young's modulus of monopile (GPa)	210
Embedded length of monopile (m)	35.5

Table 2
Parameter of the soil profile.

Parameter	Finite element zone	Infinite element zone
Effective unit weight γ_s^e (kN/m^3)	10	10
Young's modulus E (MPa)	40	40
Poisson's ratio ν	0.25	0.25
Internal friction angle φ (deg)	35	/
Dilation angle ψ (deg)	5	/
Cohesion c (kPa)	0.1	/

soil. The overall FE model of the soil-monopile-tower system is shown in Fig. 1. The interaction between soil and pile is modeled by ABAQUS built-in small-sliding, surface-to-surface master/slave contact pair formulation, where the penalty method is used for tangential direction and the Lagrange multiplier method is used for normal direction.

Vibration damping is a key parameter affecting the dynamic behavior of the OWT, which generally comprises aerodynamic damping, structural damping, hydrodynamic damping, and soil damping. The soil damping comes from the soil-structure interaction and mainly includes material damping and wave radiation damping. Considering the large-amplitude wave and wind loading concentrate on the low-frequency range, the energy dissipated by the wave radiation can be neglected and only material damping of the soil is taken into account in this study. Based on the damping estimation from the past papers [7,27–29], 6.21% is adopted for the damping ratio of the fore-aft direction in the present study, which is used to calculate the mass and stiffness coefficients in Rayleigh damping.

2.2. Foundation modeling

This study focuses on the influence of the foundation model on the dynamic performance of OWTs, where three typical foundation models are considered for analysis. The apparent fixity model and distributed spring model are commonly applied in the engineering practice, while the finite element model is more often considered for some research on the complex soil behavior and soil-pile interaction. The three models are illustrated in Fig. 2.

2.2.1. Apparent fixity model

In the apparent fixity model, the pile is fixed at an effective depth below the mudline to incorporate the clamping effect of the soil. In engineering practice, designers often use this model as preliminary dynamic analysis of offshore structures owing to its simplicity. The determination of the only model parameter effective fixity depth relies on the soil condition and pile dimension. The general suggested value for the offshore structure ranges between 3.5 and 8 times the pile diameter D [11], while the lower value range 3.3D to 3.7D is better in agreement with the monopile behavior with larger pile diameter based on Kuhn [12] and Zaaijer [13] research. Therefore, 3.5D is selected for the effective fixity depth in this study.

2.2.2. Distributed spring model

In the distributed spring model, the soil-structure interaction between monopile and surrounding soil is simulated via a set of lateral and vertical nonlinear springs distributing along the monopile. The p-y relationship under cyclic load recommended in API [15] and DNV [14] is adopted for lateral springs to simulate the lateral resistance of the soil, while the t-z and Q-z relationship [14,15] are used for vertical springs to consider shaft friction and end bearing capacity. The springs have a nonlinear elastic stress-strain relationship and mutual independence according to Winkler's assumption. Due to its simplicity and relative accuracy, this model is commonly applied in the oil and gas industry.

The nonlinear soil lateral resistance-deflection (p-y) relationships for sand may be approximated at depth z as:

$$P = A \times p_u \times \tanh\left[\frac{k \times z}{A \times p_u} \times y\right] \tag{1}$$

where P is soil resistance in kN/m, y is soil deflection in m, $A = 0.9$ for cyclic loading, k is the initial modulus of subgrade reaction in kN/m^3, determined as a function of internal frication angle, p_u is ultimate bearing capacity, is defined as:

$$\begin{aligned} p_{us} &= (C_1 \times z + C_2 \times D) \times \gamma_s^e \times z \\ p_{ud} &= C_3 \times D \times \gamma_s^e \times z \end{aligned} \tag{2}$$

where p_{us} for shallow depth, p_{ud} for deep depth, γ_s^e is effective soil weight, D is pile diameter, C_1, C_2, and C_3 are coefficients determined

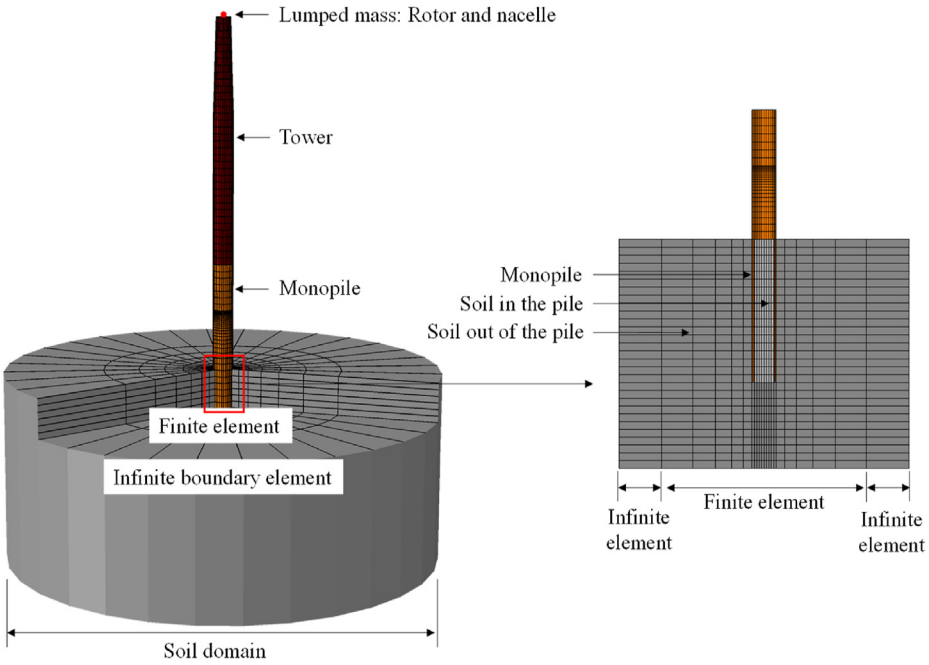

Fig. 1. 3D FE model.

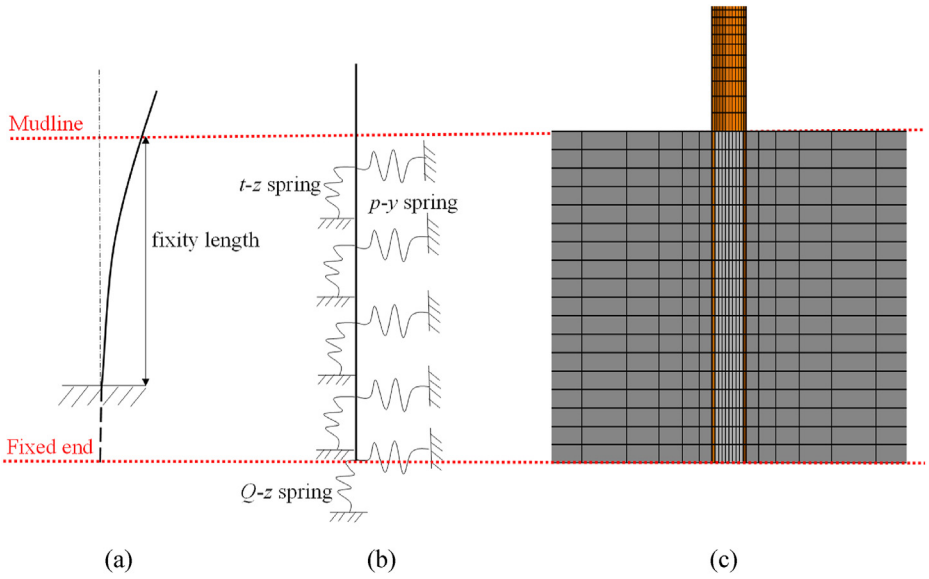

Fig. 2. Foundation models: (a) apparent fixity model; (b) distributed spring model; (c) FE model of the soil-pile system.

as a function of internal friction angle.

2.2.3. Finite element model of the soil-pile system

In the finite element model of the soil-pile system, the overall model consisted of the monopile-tower system and soil is established, where some elastoplastic material model and contact algorithm are used to simulate the characteristic response of monopile foundation subject to more complex environmental loading. In order to eliminate the artificial boundary effect resulting from the introduction of the solid element soil model, the dimension of the soil domain is selected through the trial run to verify its adequacy. Some empirical dimensional parameters can be used as reference, for instance, Haiderali [19] constructed a large soil zone with a height of 1.6*L* (*L* is the embedded length of monopile) and a diameter of 20*D* (*D* is the diameter of monopile), and Ahmed [20] modeled a soil domain of 15*D* in diameter and 1.67*L* in depth. Compared to the semi-empirical *p-y* method developed for small-diameter piles, this foundation model can be better applicable to the monopile with a larger diameter and encompass the continuum effect associated with the foundation. In the meanwhile, the establishment of a solid soil domain provides more possibilities to take complicated soil behaviors under monotonic and cyclic loading into account. The soil domain in this study has 10*D* in width and 1.6*L* in depth, surrounding with the infinite element zone to avoid the boundary effect.

2.3. Types of loading on the structure

The cost-effective and durable design of OWT requires the accurate prediction of its response to complex environmental conditions, which relies on the appropriate modeling of the combined action of incident wind and wave. In this study, the dynamic simulations in the time domain are used to obtain the response of the offshore wind turbine under these external vibrations, and the relevant simulation techniques characterizing the stochastic nature of wind and wave loading are presented in this section.

2.3.1. Stochastic wind load

The wind loading acting on the offshore wind turbine can be divided into two components, namely the loading on the tower and the loading on the blades. For the former, the wind loading at different location z can be expressed as:

$$F_{tower}(z) = \frac{1}{2} C_{dt} A(z) \rho_{air} u(z)^2 \tag{3}$$

where C_{dt} is the drag coefficient, 1.2, $A(z)$ is the area associated with the location z and u is the total wind velocity, ρ_{air} is the air density, 1.225 kg/m^3.

For the loading on the blade, this study only considers the parked condition of the offshore wind turbine, and the thrust force on the blade is computed using the blade element momentum (BEM) method. In terms of the BEM approach, the blade is divided up into N elements and the overall resultant force is obtained by numerical integration along the blade span. For each blade element, the resultant force F is decomposed into lift force F_L and drag force F_D, as shown in Fig. 3, which can be computed as follow:

$$\begin{aligned} F_L &= 0.5 \rho_{air} V_{rel}^2 c \Delta r C_L \\ F_D &= 0.5 \rho_{air} V_{rel}^2 c \Delta r C_D \end{aligned} \tag{4}$$

where C_L is the lift coefficient, C_D is the drag coefficient, c and Δr is the chord length and the radial length of the blade element, V_{rel} is the relative wind velocity, which can be computed as:

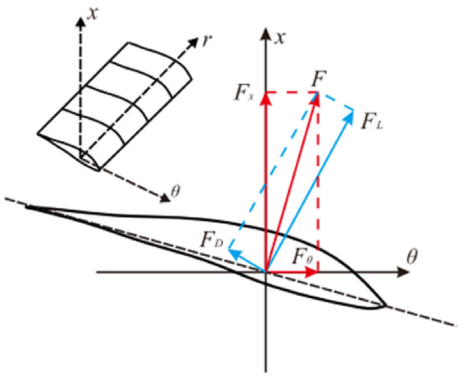

Fig. 3. Forces on each blade element.

$$V_{\mathrm{rel}} = \sqrt{V_x^2 + (\Omega r - V_\theta)^2} \tag{5}$$

where V_x and V_θ are the axial velocity and tangential velocity on the rotor, Ω is the angular speed of the blade, r is the radial distance between the hub center and the element center. Therefore, the thrust force acting on the blade element in the axial direction can be computed as:

$$F_x = F_L \cos\varphi + F_D \sin\varphi \tag{6}$$

where φ is the relative wind angle, which can be calculated as:

$$\varphi = \tan^{-1}[V_x / (\Omega r - V_\theta)] = \theta_P + \gamma + \alpha \tag{7}$$

where θ_p is the blade pitch angle, γ is the blade twist angle, and α is the angle of the attack.

The wind velocity consists of two components, namely the constant mean wind velocity and the fluctuating wind velocity. The former $\overline{u}$ at position z in the neutral ABL (atmospheric boundary layer) can be expressed as:

$$\overline{u}(z) = \frac{u^*}{\kappa}\ln\left(\frac{z}{z_0}\right) \tag{8}$$

where u^* is the friction velocity, κ is the Von Karman constant, z_0 is the roughness height. In the present study, the mean wind velocity at the hub height is taken as 8 m/s, and the roughness height is 0.005.

The fluctuating wind velocity field along the long-span tower is simulated using the spectral representation method [30,31]. With the coherence between three dimensions ignored, the problem can be simplified as a one-dimensional multivariate stochastic process $\{f(t)\}$ with n components $f_1(t), f_2(t), \ldots, f_n(t)$, which can be simulated by:

$$\begin{aligned} f_j(t) &= \sqrt{2(\Delta\omega)}\sum_{m=1}^{j}\sum_{l=1}^{N}|H_{jm}(\omega_{ml})|\cos(\omega_{ml}t - \theta_{jm}(\omega_{ml}) + \Phi_{ml}) \\ \theta_{jm}(\omega) &= \tan^{-1}\left\{\frac{\mathrm{Im}[H_{jm}(\omega)]}{\mathrm{Re}[H_{jm}(\omega)]}\right\} \\ \omega_{ml} &= (l-1)\Delta\omega + \frac{m}{n}\Delta\omega \\ j &= 1,2,\ldots n \end{aligned} \tag{9}$$

where N is a large number, $\Delta\omega = (\omega_{\mathrm{up}}/N)$, ω_{up} is the upper cutoff frequency, $\Phi_{1l}, \ldots, \Phi_{jl}$ are random sequences distributing uniformly in $[0, 2\pi]$, $H(\omega)$ is defined as the Cholesky's decomposition of the cross-spectral density matrix $\mathbf{S}^0(\omega)$

$$\mathbf{S}^0(\omega) = \mathbf{H}(\omega)\mathbf{H}^{T^*}(\omega) \tag{10}$$

and

$$\begin{aligned} &S_{11}^0(\omega) = S_{22}^0(\omega) = \ldots = S_{nn}^0(\omega) = S(\omega) \\ &S_{jm}^0(\omega) = \sqrt{S_{jj}^0 S_{mm}^0}\,Coh(\Delta_{jm},\omega) = S(\omega)Coh(\Delta_{jm},\omega) \\ &j,m = 1,2,\ldots,n \end{aligned} \tag{11}$$

where Δ_{jm} is the distance between positions j and m, $Coh(\Delta_{jm}, \omega)$ is the coherence function between positions j and m, which can be computed as:

$$Coh(\Delta_{jm},\omega) = \exp\left(-\frac{\lambda\omega\Delta_{jm}}{2\pi u(z)}\right) \tag{12}$$

where λ is the co-coherence decay coefficient.

In this study, we only consider the upstream turbine and ignore the rotational sampling turbulence resulting from the rotation of the rotor blades. Kaimal spectrum is taken as the stochastic wind spectrum $S(\omega)$ [32], as shown in Fig. 4, which is defined as

$$\begin{aligned} S(f,z) &= \frac{u_*^2}{f}\frac{200c}{(1+50c)^{5/3}} \\ c &= fz/\overline{u}(z) \\ f &= 2\pi\omega \end{aligned} \tag{13}$$

2.3.2. Stochastic wave load

The wave loading on the monopile is estimated using the Morison equation, the wave force per unit length at depth z [14,15], which are expressed as follows:

$$f = \frac{1}{2}C_D\rho D(u-\dot{q})|u-\dot{q}| + \left[C_M\frac{\pi D^2}{4}\rho a - (C_M-1)\frac{\pi D^2}{4}\rho\ddot{q}\right] \tag{14}$$

Where C_D and C_M are the drag and inertia coefficients, ρ is water density, D is the diameter of monopile, $\dot{q}$ and $\ddot{q}$ are the horizontal velocity and acceleration of structure respectively, u and a are the velocity and acceleration of water particle in the horizontal direction at depth z, which can be calculated based on the sea surface elevation η. The most common model in the current practice to characterize stochastic wave is limited to linear wave theory, where the sea surface elevation η can be expressed as:

$$\eta(t) = \sum_{m=1}^{N} A_m\cos(w_m t + \varphi_m) \tag{15}$$

where w_m is the frequency of the mth component, A_m is the Rayleigh distributed amplitudes: $E[A_m^2] = 2S(w_m)\Delta w$, φ_m is the random phase uniformly distributed over $[0,2\ \pi]$. The corresponding velocity u and acceleration a at depth z can be represented as:

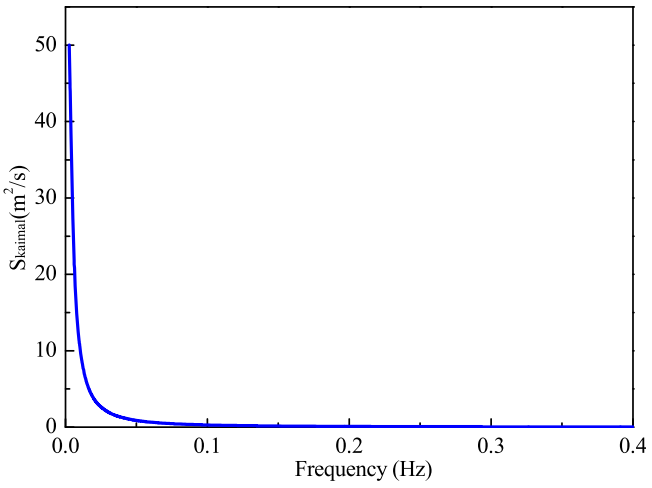

Fig. 4. Kaimal wind spectrum.

$$u(z,t)=\sum_{m=1}^{N}A_m w_m\frac{\cosh(k_m(h+z))}{\sinh(k_m d)}\cos(w_m t+\varphi_m)$$
$$a(z,t)=-\sum_{m=1}^{N}A_m {w_m}^2\frac{\cosh(k_m(h+z))}{\sinh(k_m d)}\sin(w_m t+\varphi_m) \quad (16)$$

where k_m is wave number, h is water depth, taking 18.2 m according to the site investigation in the present study.

In the current practice, the JONSWAP spectrum is often used to calculate the sea surface elevation in severe conditions. It is a typical single-peak spectrum and is mainly proposed in accordance with the developing sea state [14], as shown in Fig. 5.

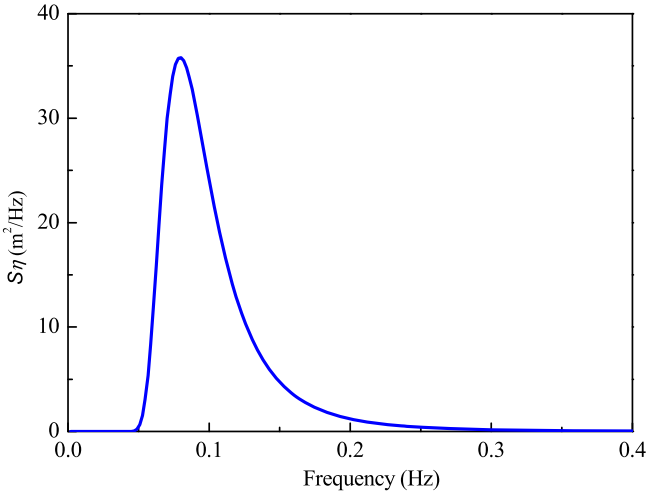

Fig. 5. JONSWAP wave spectrum.

$$S(f)=C(\gamma)\cdot 0.3125\cdot {H_s}^2\cdot {f_p}^4\cdot f^{-5}\exp\left(-1.25\left(\frac{f_p}{f}\right)^4\right)\cdot\gamma^{\alpha} \quad (17)$$

where $f_p = 1/T_p$. T_p and H_s denote the peak wave period and the significant wave height, respectively. $T_p = 12.58$ s and $H_s = 5.64$ m are obtained from the site measurement. f is wave frequency, γ is peak-shape parameter, σ is the spectral width factor, and $C(\gamma)$ is normalizing factor.

3. Model verification

The apparent fixity model and distributed spring model have been widely validated and used in the previous researches, while the employed modeling approach of finite element model of the soil-pile system in this study needs to be further verified considering the complexity of modelling procedures and uncertainty of related modelling details. The fundamental frequency of offshore wind turbines serves as a primary indicator to capture the dynamic characteristics of the structure, which can be used to initially verify the numerical capability of the FE model. To verify the accuracy and efficacy of the FE models mentioned above, three real-world offshore wind turbines are selected from the literature with detailed structural and soil data [16], which are outlined in Table 3. To fully take the variation of the dynamic performance concerning the size of the wind turbine into account, the monopile diameter of three types of wind turbine ranges from 3.2 m to 6 m. In the meanwhile, the differences in soil behaviors between sand and clay are included to assess the applicability of the foundation modeling approach.

The actual measurement of the first natural frequency coming from site investigation is also obtained for reference. Based on these data, numerical models are developed and solved for fundamental natural frequency, which is summarized in Table 4. The results show that predicted fundamental frequencies agree well with the site measurements, lending to the good applicability of the numerical model to analyze the dynamic behavior of offshore wind turbines (see Table 5).

Table 3
Structural data of OWT.

Offshore wind turbine	Walney 1	Lely A2	North Hoyle
Tower height (m)	67.3	37.9	67
Tower top diameter (m)	3	1.9	2.3
Tower bottom diameter (m)	5	3.2	4
Tower wall thickness (mm)	40	13	35
Young's modulus of tower material (GPa)	210	210	210
Top mass (t)	234.5	32	100
Monopile diameter (m)	6	3.2	4
Monopile wall thickness (mm)	80	35	50
Young's modulus of monopile material (GPa)	210	210	210
Monopile depth (m)	23.5	13.5	33
Shear modulus of the soil (MPa)	70	140	230
Poisson's ratio of the soil	0.4	0.4	0.4
Young's modulus of the soil (MPa)	196	392	644

Table 4
Site condition and fundamental frequency of OWT.

Offshore wind turbine	Walney 1	Lely A2	North Hoyle
Soil condition at the site	sand layers	sand and clay layers	sand and clay layers
Measured fundamental frequency (Hz)	0.35	0.64	0.35
Predicted fundamental frequency (FE model of the soil-pile system) (Hz)	0.31	0.70	0.34

4. Results and discussions

4.1. Dynamic responses based on three numerical foundation models

The offshore wind turbines are dynamically sensitive structures due to the slenderness of the system, which means the fatigue failure is critical during their service life. To minimize the development of fatigue damage, it is essential to avoid dynamic amplification owing to the resonance of the structure. Therefore, the first natural frequency of the structure should not coincide with the excitation frequencies coming from wind and wave, which requires a reliable estimation of this parameter in the design phase. In this section, the natural frequency for each foundation model is firstly obtained based on the modal analysis and normalized with the result of the FE model of the soil-pile system, as given in Table 6. It's observed that the natural frequency of the offshore wind turbine marginally changes for three foundation models, with the maximum difference below 3%. The natural frequency of the apparent fixity model is slightly smaller than that of the FE model of the soil-pile system, while the result of distributed spring model is almost the same. These preliminary results of the natural frequency suggest that the empirical apparent fixity model underestimates the foundation stiffness, while the distributed spring model can give a relatively accurate prediction of the foundation stiffness in this case.

To gain further insight into the difference in dynamic performance among the three foundation models, the time-domain analysis is carried out with the combined wind and wave loading taken into account. The incident wave significant height and peak period are 5.64 m and 12.58 s, respectively, and the incident wind velocity at the hub height of the offshore wind turbine is 8 m/s. The dynamic responses including the horizontal displacement and acceleration at the tower top and the shear force at the mudline are picked for the comparison. Fig. 6 shows the comparison of the amplitude spectra of the dynamic performance between three foundation models. As shown in Fig. 6(a), two obvious peaks appear close to 0.08 Hz and 0.30 Hz, which corresponds to the peak frequency of the wave spectrum and the natural frequency of the offshore wind turbine, respectively. Compared with the FE model of the soil-pile system, the apparent fixity model simultaneously increases the low-frequency and high-frequency component near two peak frequencies significantly, and the displacement response of the distributed spring model has a little higher energy in these two frequency ranges. The power spectrum of the acceleration at the tower top shows a significant crest around the natural frequency of the structure (Fig. 6(b)), with the highest peak for the apparent fixity model and slightly more energy contained in the high-frequency domain for the distributed spring model. Fig. 6(c) shows the PSDs of the internal force response at the mudline, where the dominant frequency appears at about the peak frequency of the wave spectrum. Moreover, the internal force response of the FE model of the soil-pile system has higher concentrated energy in the low-frequency zone near the peak frequency of the wave spectrum in comparison with the other two foundation models.

To compare the results quantitatively, the relevant statistics, the root mean square (RMS) and maximum, are introduced, which is defined as:

$$RMS = \sqrt{\frac{y_1^2 + y_2^2 + \ldots + y_n^2}{n}} \tag{18}$$

where y_i is the response at the time step i and n is the number of the time step. The RMS of the displacement, acceleration at the tower top, and shear force at the mudline for three foundation models are obtained and normalized with the result of the FE model of the soil-pile system. Tables 6 and 7 illustrate the maximum and the RMS of the responses, respectively. Compared with the response based on the apparent fixity model, the results of the distributed spring model are closer to the FE model of the soil-pile system. In general, the apparent fixity model and distributed spring model increase the displacement and acceleration response at the tower top, whereas reducing the internal force response at the mudline. Furthermore, the influence of the foundation model on the displacement and acceleration response is slightly more remarkable than the internal force response. The results reveal that the displacement and acceleration response at the tower top is more related to the natural frequency of the response, while the internal force response at the mudline is dominated by the peak frequency of the wave spectrum.

Table 5
Predicted natural frequencies for three foundation models.

Foundation model	Natural frequency (Hz)	
	Absolute value	Normalized value
Apparent fixity model	0.29	0.97
Distributed spring model	0.30	1
FE model of soil-pile system	0.30	1

4.2. Parametric studies of foundation stiffness

Considering the engineering practice where the design parameters range within a certain interval, a parametric analysis is further carried out to investigate their influence on the dynamic performance of the offshore wind turbine, especially with respect to different foundation models. This section involves discussions on soil densification, pile diameter, pile thickness, and pile penetration depth.

Table 6
Maximum dynamic response.

Foundation model	u_{max} (m)	Normlized u_{max}	a_{max} (m^2/s)	Normalized a_{max}	F_{max} (kN)	Normalized F_{max}
Apparent fixity model	0.065	1.121	0.118	1.283	826.000	0.943
Distributed spring model	0.060	1.034	0.118	1.283	823.000	0.940
FE model of soil-pile system	0.058	1	0.092	1	875.575	1

4.2.1. Effect of soil densification

Owing to the long period of exposure to cyclic wind and wave loading, a truncated cone-shaped densified zone will be observed along the pile shaft of the offshore wind turbine [33], which may impose a notable impact on the elastic modulus and the effective unit weight of the sand. To examine the influence of the soil densification, a series of calculations are conducted using the FE model and distributed spring model, considering parameters for the densified soil (Table 8) [22], while the dynamic performance of the fixity model remains the same regardless of the soil condition. The fundamental frequencies for two soil conditions are obtained as shown in Table 9. It is observed that the natural frequency of the distributed spring model is more or less the same for two soil conditions, while the soil densification increases the natural frequency of the FE model of the soil-pile system by about 3.3%.

Fig. 7 shows the PSDs of the displacement response for two soil conditions, respectively. Considering the distributed spring model in Fig. 7(a), the minor difference can be observed in the power spectral density of the displacement response, whereas soil densification somewhat suppresses two primary peaks at about the peak frequency of the wave spectrum and the natural frequency of the structure for FE model of the soil-pile system (Fig. 7(b)). On the other hand, shear force PSDs for two soil conditions in Fig. 8 exhibits insignificant differences for both distributed spring model and the FE model of the soil-pile system. To more clearly obtain the quantitative characteristics of the dynamic response for two soil conditions, Tables 10 and 11 present the RMS of displacement and shear force response, respectively (the difference indicates the variation as compared with the original soil condition). There appears to be a trend that an increase in soil effective unit weight and elastic modulus resulting from the soil densification leads to a decrease in the displacement acceleration response for the FE model of soil-pile system, their influence on the distributed spring model is however insignificant. Furthermore, the internal force response varies slightly with the soil conditions, no matter for distributed spring model and FE model of the soil-pile system. These results suggest that the apparent fixity model and distributed spring model miss the influence of soil condition on the displacement response which can be characterized in the FE model of the soil-pile system.

4.2.2. Effect of pile diameter

The pile diameter is a key parameter in the design phase of the offshore wind turbine, which is determined based on a compromise between the dynamic performance of the structure and manufacturing cost. To investigate its effect, three different pile diameters $D = 5$ m, 5.5 m, and 6 m are considered in the present study with other parameters unchanged. Shown in Table 12 are the natural frequency for three pile diameters considering three foundation models (the percentage in the bracket indicates the variation as compared with pile diameter $D = 6$ m). Generally, a similar tendency that an increase of the natural frequency with the increasing pile diameter is observed for all three foundation models, among which the greatest influence occurs on the apparent fixity model, while the degree of variation for the other two foundation models is modest.

Fig. 9 shows the PSDs of the displacement response for three pile diameters, respectively. Note that a similar right shift of the high-frequency peak with the increasing pile diameter appears regardless of the foundation modeling approach. However, the peak energy for the apparent fixity model sees a pronounced reduction with the increasing pile diameter, while those for distributed spring model and FE model of the soil-pile system experience a relatively modest trend, especially for the larger diameter. These phenomena can be explained by the reason that

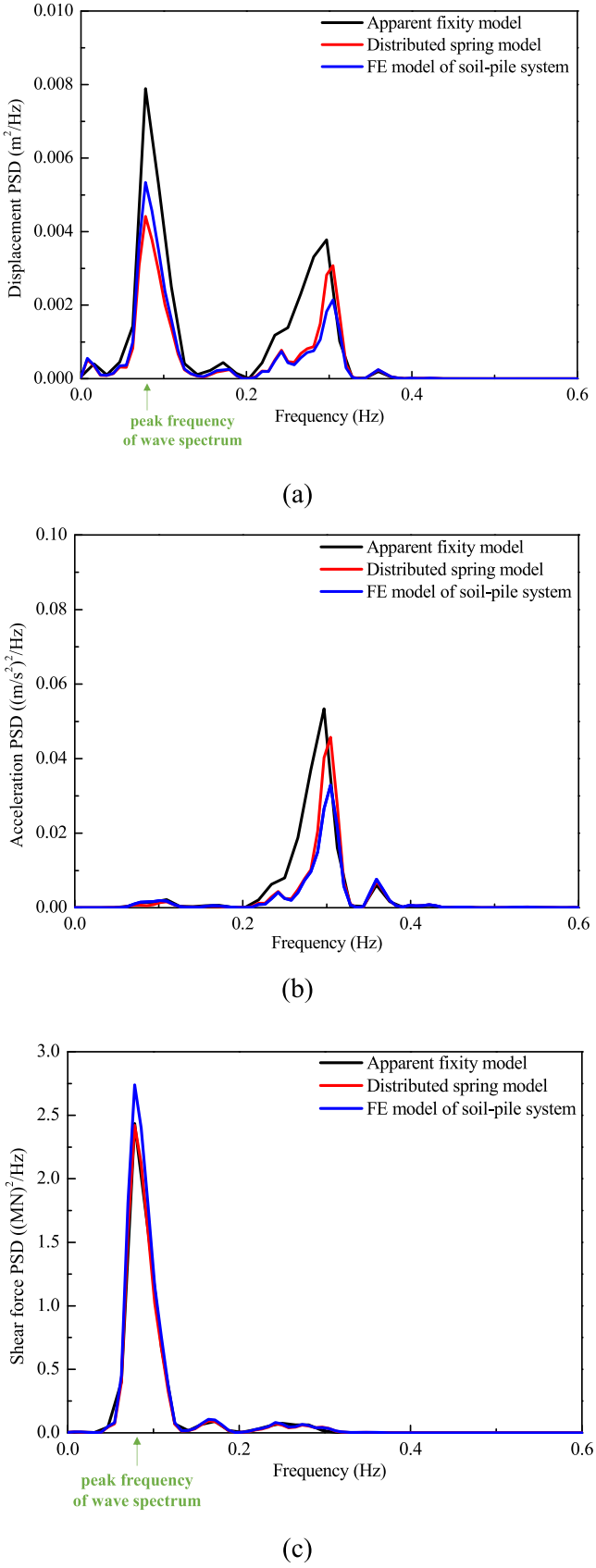

Fig. 6. Power spectral densities (PSDs) of the structural response: (a) displacement at the tower top; (b) acceleration at the tower top; (c) shear force at the mudline.

Table 7
RMS of dynamic response.

Foundation model	u_{rms} (m)	Normalized u_{rms}	a_{rms} (m^2/s)	Normalized a_{rms}	F_{rms} (kN)	Normalized F_{rms}
Apparent fixity model	0.024	1.200	0.040	1.333	214.863	0.946
Distributed spring model	0.020	1	0.034	1.133	213.718	0.941
FE model of soil-pile system	0.020	1	0.030	1	227.079	1

Table 8
Soil parameter of original and densified soil.

Parameter	Original soil	Densified soil
Effective unit weight γ_s^e (kN/m^3)	10	11
Young's modulus E (MPa)	40	60
Poisson's ratio υ	0.25	0.25
Internal friction angle φ (deg)	35	35
Dilation angle ψ (deg)	5	5
Cohesion c (kPa)	0.1	0.1

Table 9
Predicted natural frequencies of two soil conditions.

Soil condition	Apparent fixity model	Distributed spring model	FE model
Original soil	0.29 Hz	0.30 Hz	0.30 Hz
Densified soil	0.29 Hz	0.30 Hz	0.31 Hz
Difference	0	0	3.3%

the distributed spring model and FE model of soil-pile system can incorporate the variation of soil constraint resulting from the pile diameter, which is ignored by the apparent fixity model. As for the shear force PSDs, the first peak energy close to the peak frequency of the wave spectrum observes a slight increase as the pile diameter rises for the apparent fixity model and distributed spring model, while that for FE model of the soil-pile system is almost not affected by the pile diameter. A more comprehensive quantitative comparison is conducted on the RMS of the displacement and shear force response for three foundation models, as shown in Tables 13 and 14. The displacement response falls substantially with pile diameter, especially for the small diameter, whereas a more modest variation rate is observed for the shear force response. Moreover, the RMS of the displacement response for distributed spring model and FE model of soil-pile system is almost the same, which is consistent with the PSDs distribution. Note that shear force response for the FE model of soil-pile system presents an opposite trend to the other two foundation models, which can result from the difference of low-frequency peak energy at about the wave peak frequency owing to the effect of soil-plugging [34,35] in the FE model of the soil-pile system (see Fig. 10).

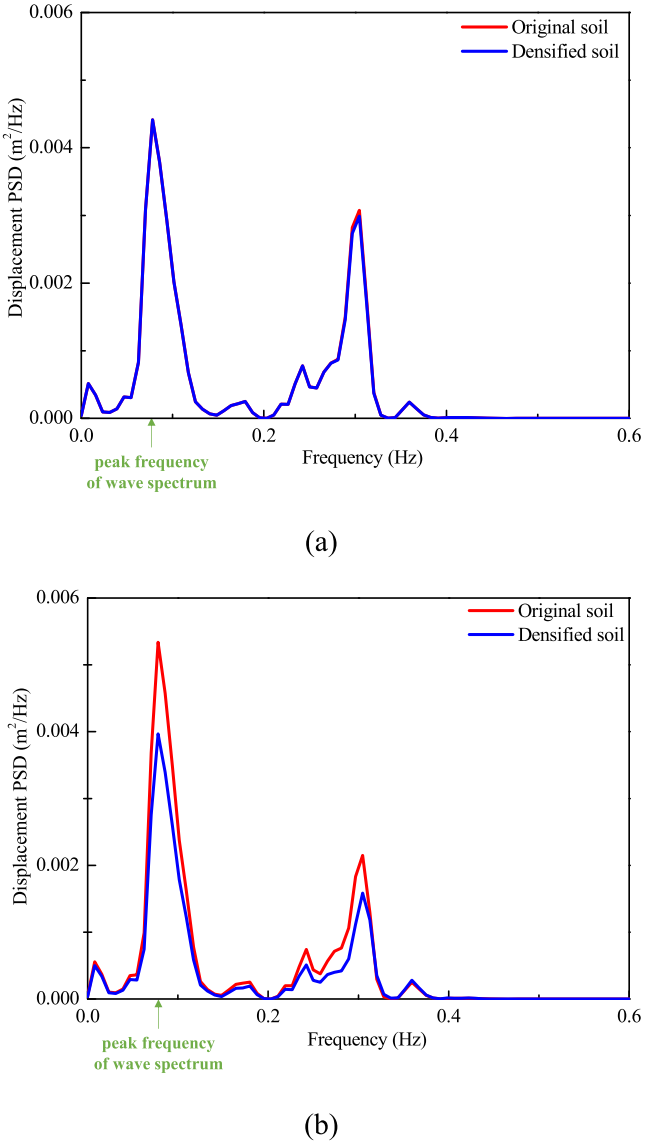

Fig. 7. Displacement PSDs for two soil conditions: (a) distributed spring model; (b) FE model of soil-pile system.

4.2.3. *Effect of pile thickness*

Another key design parameter affecting the dynamic performance of the structure is pile thickness. Considering the appropriate ratio of the pile thickness and diameter ranging from 1:50 and 1:80 [36,37] and the pile diameter $D = 6$ m in the present study, the pile thickness $t = 0.08$ m, 0.09 m, and 0.1 m are selected for comparison. Table 15 demonstrates the variation of the natural frequency with the pile thickness for three foundation models. It is obvious that the natural frequency of the structure generally rises with the pile thickness, among which the rate of change for the apparent fixity model appears more remarkable than the FE model soil-pile system, while the distributed spring model is placed in the middle.

The power spectrum of the displacement response with pile thickness for three foundation models is illustrated in Fig. 11. Generally, the low-frequency peak near the peak frequency of the wave spectrum sees an obvious drop with the pile thickness for all

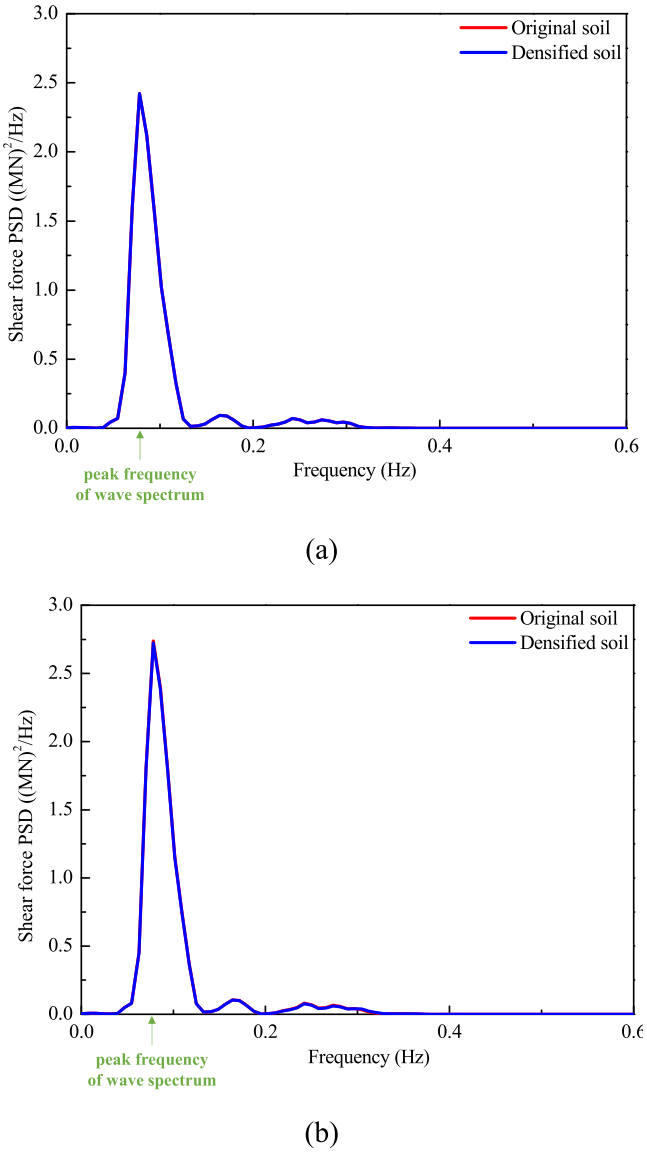

Fig. 8. Shear force PSDs for two soil conditions: (a) distributed spring model; (b) FE model of soil-pile system.

Table 10
RMS of displacement response.

Soil condition	Apparent fixity model	Distributed spring model	FE model
Original soil	0.024 m	0.020 m	0.020 m
Densified soil	0.024 m	0.020 m	0.018 m
Difference	0	0	−10.00%

Table 11
RMS of shear force response.

Soil condition	Apparent fixity model	Distributed spring model	FE model
Original soil	214.863 kN	213.718 kN	227.079 kN
Densified soil	214.863 kN	213.743 kN	226.115 kN
Difference	0	0.01%	−0.42%

three foundation models, among which the apparent fixity model exhibits the sharpest variation. As far as the high-frequency component is concerned, a right shift of the secondary peak is observed commensurate with the variation of the natural frequency of the structure. Furthermore, the apparent fixity model is least sensitive to the pile thickness and experiences a modest fall in peak value with the increasing pile thickness, while this trend is significant for the distributed spring model and the FE model of the soil-pile system. Based on the PSDs of the shear response in Fig. 12, note that pile thickness almost imposes no impact on the shear response, except for the minor difference near the peak frequency of the structure. Tables 16 and 17 further compare the statistics of time-domain analysis for the displacement and shear force response, respectively. It is observed that an increase in pile thickness results in a reduction of the displacement response no matter for different foundation models, among which the effect is more pronounced for the apparent fixity model but weakened for the other two foundation models, especially for the response of distributed spring model. On the other hand, the difference concerning the RMS of the shear force response between varying pile thickness further illustrates that the internal force response almost remains the same regardless of the variation of the pile thickness.

4.2.4. Effect of pile penetration depth

The pile penetration depth plays an important role in the performance of offshore wind turbines, especially for the stability of the structure. To investigate its influence and the sensitivity of different foundation models to this parameter, dynamic responses are obtained for three penetration depths $L = 24$ m, 35.5 m, and 48 m. Owing to the simplification of the fixed end for the apparent fixity model, only the distributed spring model and FE model of soil-pile system are discussed in this section. According to the natural frequency shown in Table 18, the elongation of pile embedded depth brings about the increase of natural frequency with a decreasing rate.

Considering the displacement response, as shown in Fig. 13, the two primary peaks at around the peak frequency of the wave spectrum and the natural frequency of the structure both fall remarkably for two foundation models when the penetration depth varies from 24 m to 35.5 m. Moreover, its influence on the low-frequency peak is slightly greater for the FE model of soil-pile system than the distributed spring model. When it comes to the case where the pile penetration depth varies from 35.5 m to 48 m, the two PSD distributions almost overlap no matter for the distributed spring model and FE model of the soil-pile system. As for the PSDs of the shear force response in Fig. 14, all three lines almost overlap for three penetration depths regardless of the foundation model. A quantitative comparison is illustrated in Table 19 and 20. Constant displacement responses remain when the penetration is larger than 35.5 m after a reduction with the penetration depth ranging from 24 m to 35.5 m for the distributed spring model. A similar trend occurs for the displacement response of the FE model of the soil-pile system. The shear force response only fluctuates slightly with the varying pile penetration depth, which can be ignored (see Table 20).

4.2.5. Comprehensive dimensionless index of foundation stiffness

Previous studies have shown that there are distinct differences in dynamic response for different foundation stiffness, specifically the rigid or flexible fashion in which the foundation behaves [38–40]. According to the parametric analysis mentioned above,

Table 12
Predicted natural frequencies for three pile diameters.

Pile diameter	Apparent fixity model	Distributed spring model	FE model
5 m	0.24 Hz (−17.2%)	0.26 Hz (−13.3%)	0.26 Hz (−13.3%)
5.5 m	0.26 Hz (−10.3%)	0.28 Hz (−6.7%)	0.28 Hz (−6.7%)
6 m	0.29 Hz	0.30 Hz	0.30 Hz

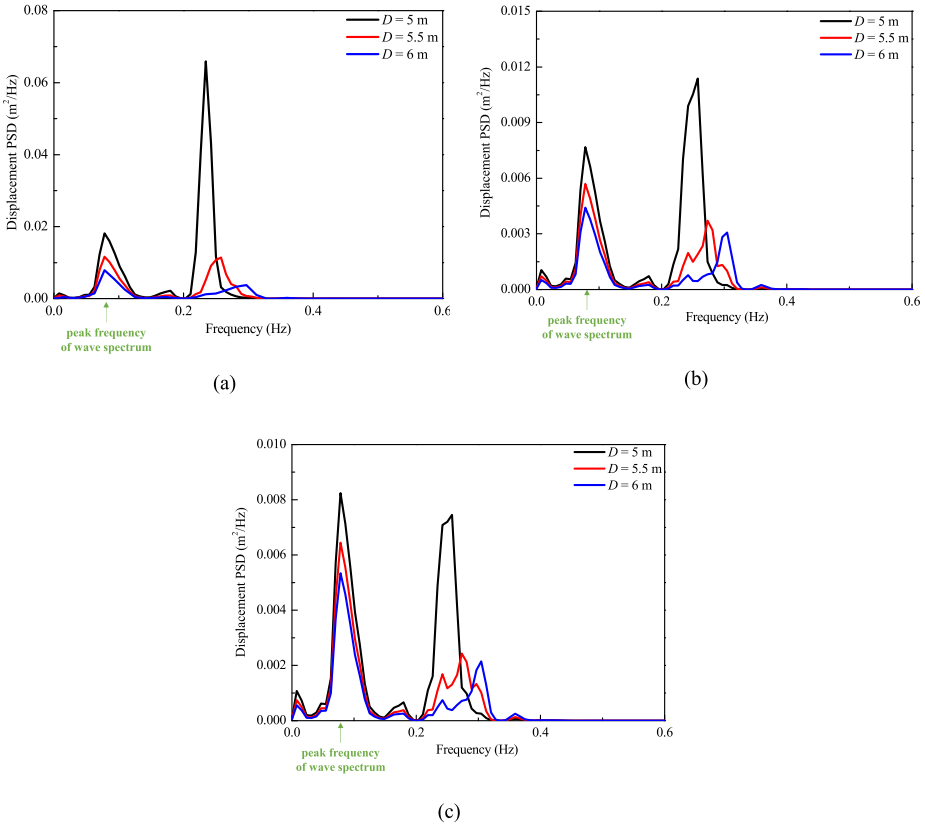

Fig. 9. Displacement PSDs for three pile diameters: (a) apparent fixity model; (b) distributed spring model; (c) FE model of soil-pile system.

the effect of the soil condition and pile penetration depth on the foundation stiffness are both missed for the apparent fixity model. Therefore, to investigate the sensitivity of all three foundation models to the different foundation stiffness comprehensively, the results of the parametric analysis in terms of pile diameter and thickness are adopted. A dimensionless index S describing the pile foundation behavior [41] is introduced in this section to incorporate the effects of the pile diameter and thickness for three foundation models, which can be expressed as:

$$S = \frac{E_s L^4}{E_p I_p} \tag{19}$$

where E_s and E_p are the elastic moduli of the soil and pile, respectively, L is the pile penetration depth, and I_p is the moment of inertia of the pile, which satisfies

$$I_p = \frac{\pi\left(D^4 - (D-2t)^4\right)}{64} \tag{20}$$

Fig. 15 shows the variation of the dynamic performance with the change of the foundation stiffness resulting from the varying pile diameter D (square symbol) and thickness t (triangle symbol), respectively. As shown in Fig. 18(a), in general, the natural frequency is more sensitive to the change of the foundation stiffness due to the pile diameter. On the other hand, the natural frequency of the FE model of soil-pile system is less sensitive to the foundation stiffness as compared to the apparent fixity model and distributed spring model. As far as the displacement response in Fig. 15(b), the degree of influence of the foundation stiffness coming from the pile diameter and thickness sees no obvious difference with a straight line. It can also be seen that the effect of foundation stiffness on the displacement response is more pronounced for the apparent fixity model, and the difference between distributed spring model and FE model of the soil-pile system is however insignificant. Fig. 15(c) shows that no obvious variation of the shear force response with the varying foundation stiffness due to the change of the pile thickness. On the contrary, an opposite trend with the foundation stiffness caused by the pile diameter can be observed for different foundation models, i.e., nearly constant for the FE model of soil-pile system and downward for the other two foundation models. To

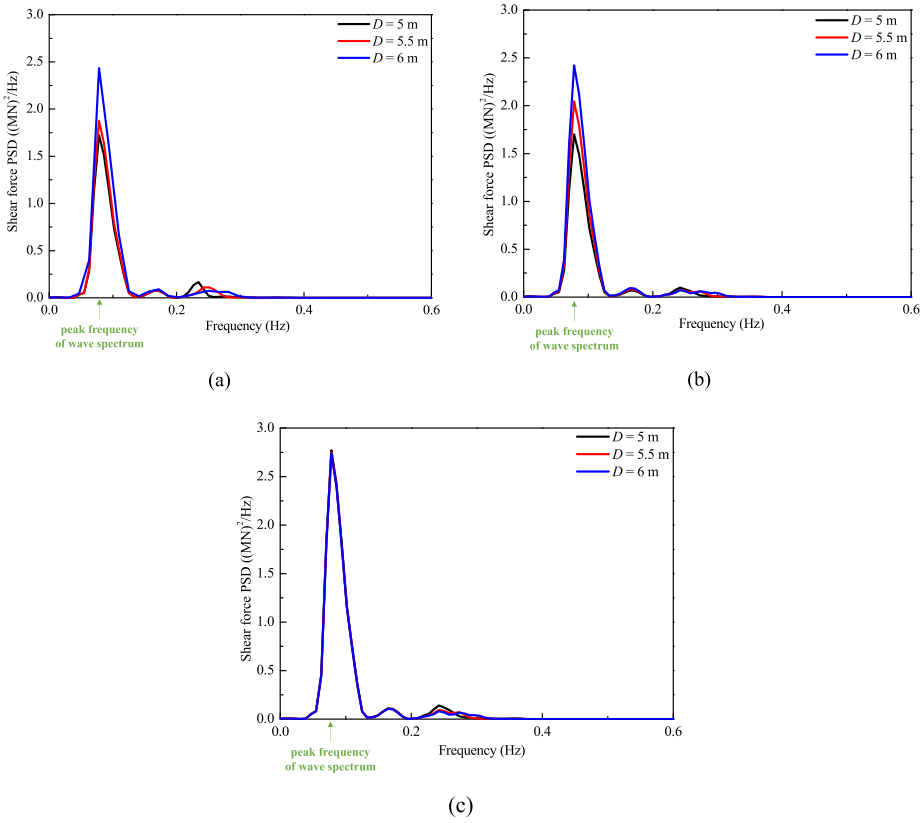

Fig. 10. Shear force PSDs for three pile diameters: (a) apparent fixity model; (b) distributed spring model; (c) FE model of soil-pile system.

Table 13
RMS of displacement response.

Pile diameter	Apparent fixity model	Distributed spring model	FE model
5 m	0.045 m (87.5%)	0.031 m (55.0%)	0.030 m (50.0%)
5.5 m	0.031 m (29.2%)	0.024 m (20.0%)	0.024 m (20.0%)
6 m	0.024 m	0.020 m	0.020 m

Table 14
RMS of shear force response.

Pile diameter	Apparent fixity model	Distributed spring model	FE model
5 m	185.096 kN (−13.9%)	181.579 kN (−15.0%)	230.914 kN (1.7%)
5.5 m	190.264 kN (−11.4%)	196.967 kN (−7.8%)	228.124 kN (0.5%)
6 m	214.862 kN	213.718 kN	227.079 kN

Table 15
Predicted natural frequencies for three pile thicknesses.

Pile thickness	Apparent fixity model	Distributed spring model	FE model
0.08 m	0.29 Hz	0.30 Hz	0.30 Hz
0.09 m	0.30 Hz (3.4%)	0.32 Hz (6.7%)	0.30 Hz
0.1 m	0.31 Hz (6.9%)	0.32 Hz (6.7%)	0.31 Hz (3.3%)

summarize, when it comes to the natural frequency, the apparent fixity model and FE model of the soil-pile model are recommended for the small foundation stiffness index, whereas the distributed spring model takes the place of the apparent fixity model gradually with the increase of the foundation stiffness index. Nevertheless, as far as the tower top displacement is concerned, the distributed spring model is always superior to the apparent fixity model regardless of the foundation stiffness, with trivial discrepancies as compared with the FE model of the soil-pile system.

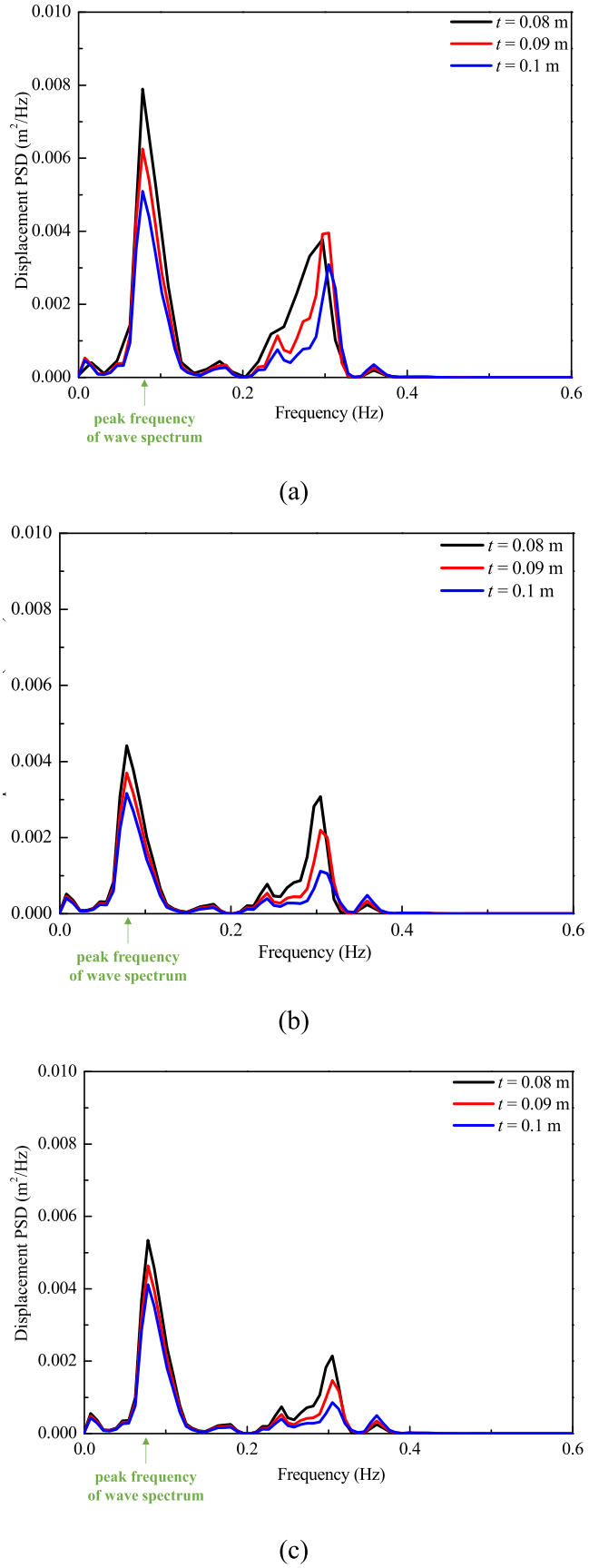

Fig. 11. Displacement PSDs for three pile thicknesses: (a) apparent fixity model; (b) distributed spring model; (c) FE model of soil-pile system.

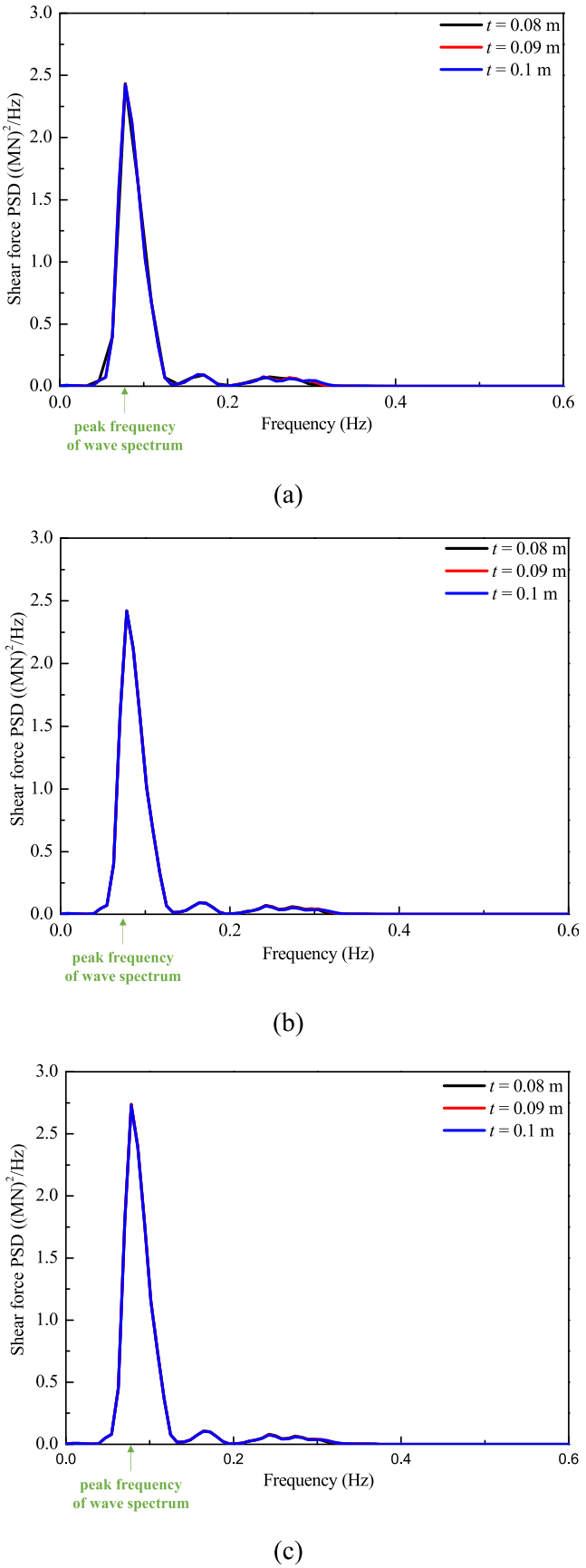

Fig. 12. Shear force PSDs for three pile thicknesses: (a) apparent fixity model; (b) distributed spring model; (c) FE model of soil-pile system.

Table 16
RMS of displacement response.

Pile thickness	Apparent fixity model	Distributed spring model	FE model
0.08 m	0.024 m	0.020 m	0.020 m
0.09 m	0.021 m (−12.5%)	0.018 m (−10.0%)	0.019 m (−5.0%)
0.1 m	0.019 m (−20.8%)	0.017 m (−15.0%)	0.017 m (−15.0%)

Table 17
RMS of shear force response.

Pile thickness	Apparent fixity model	Distributed spring model	FE model
0.08 m	214.862 kN	213.718 kN	227.079 kN
0.09 m	214.520 kN (−0.2%)	213.348 kN (−0.2%)	226.673 kN (−0.2%)
0.1 m	214.048 kN (−0.4%)	213.000 kN(-0.3%)	226.213 kN (−0.4%)

Table 18
Predicted natural frequencies for three pile penetration depths.

Penetration	Apparent fixity model	Distributed spring model	FE model
24 m	0.290 Hz	0.297 Hz (−2.3%)	0.291 Hz (−1.7%)
35.5 m	0.290 Hz	0.304 Hz	0.296 Hz
48 m	0.290 Hz	0.305 Hz (0.3%)	0.298 Hz (0.7%)

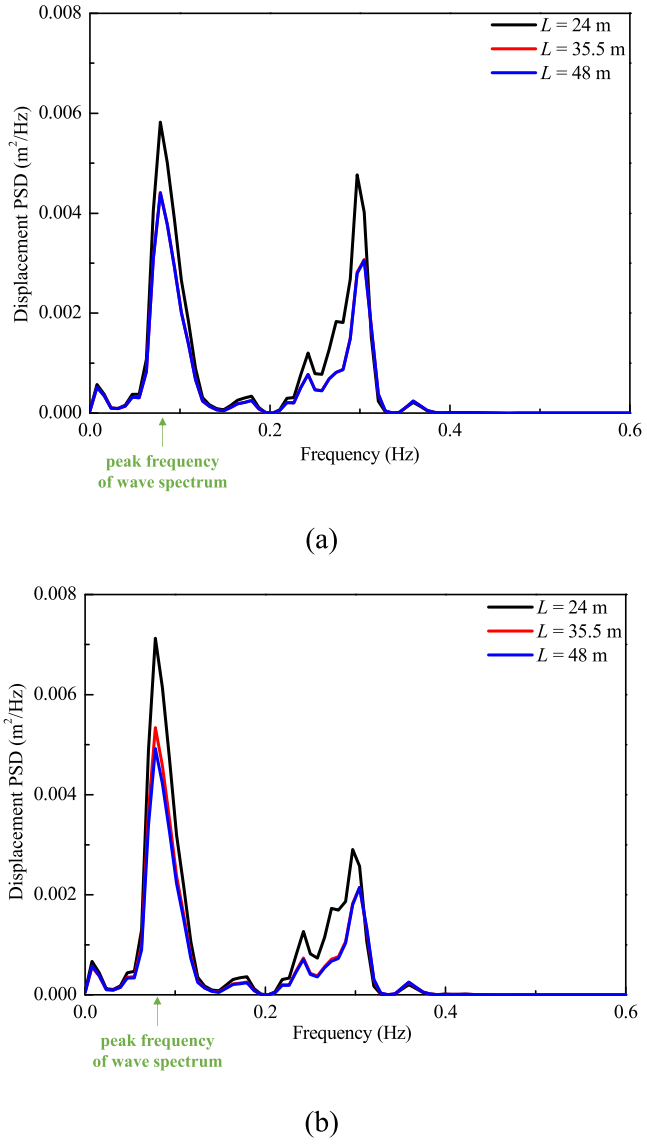

Fig. 13. Displacement PSDs for three pile penetration depths: (a) distributed spring model; (b) FE model of soil-pile system.

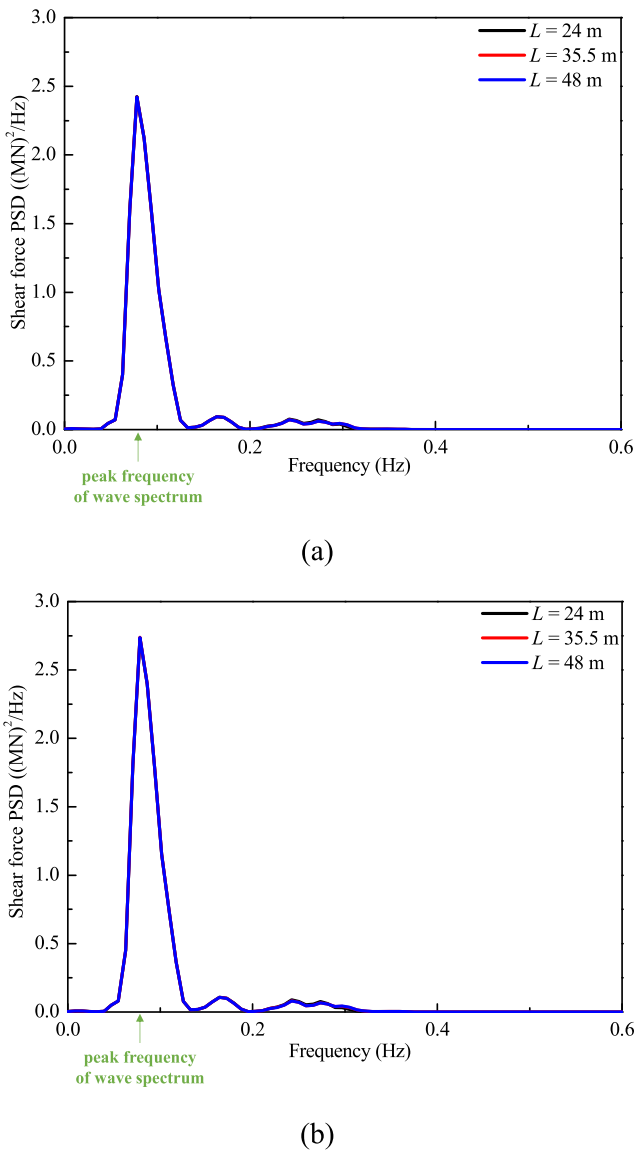

Fig. 14. Shear force PSDs for three pile penetration depths: (a) distributed spring model; (b) FE model of soil-pile system.

Table 19
RMS of displacement response.

Penetration	Apparent fixity model	Distributed spring model	FE model
24 m	0.024 m	0.022 m (10.0%)	0.022 m (10.0%)
35.5 m	0.024 m	0.020 m	0.020 m
48 m	0.024 m	0.020 m (0%)	0.020 m (0%)

Table 20
RMS of shear force response.

Penetration	Apparent fixity model	Distributed spring model	FE model
24 m	214.862 kN	214.270 kN (0.3%)	227.083 kN (0%)
35.5 m	214.862 kN	213.718 kN	227.079 kN
48 m	214.862 kN	213.725 kN (0%)	226.984 kN (0%)

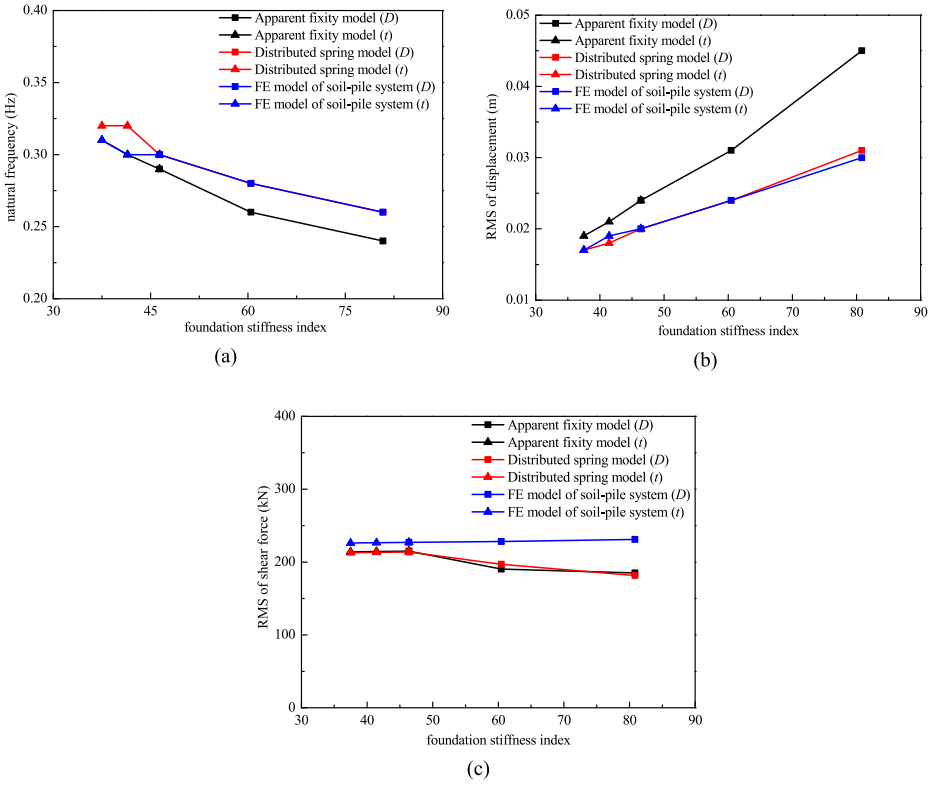

Fig. 15. Structural response for different foundation stiffnesses: (a) natural frequency; (b) displacement; (c) shear force.

5. Conclusions

The accurate estimation of the dynamic behavior of the offshore wind turbine is fundamental to its stability, operation, and performance, where the appropriate foundation modeling plays an important role. This paper carries out numerical studies on the dynamic responses of the offshore wind turbine exposed to the combined wind and wave loadings considering three foundation modeling approaches, apparent fixity model, distributed spring model, and FE model of the soil-pile system. A case study of a 5 MW offshore wind turbine supported by the monopile is conducted to systematically examine the influence of foundation modeling and then its sensitivity to different design parameters is also discussed in depth. Based on sensitivity to the proposed dimensionless foundation stiffness index in comparison with the benchmark high-fidelity FE model of the soil-pile system, recommendations on the applicability of two other simplified foundation modeling approaches, the apparent fixity model and distributed spring model, are subsequently offered. The main results are concluded as follows:

(a) Compared with the FE model of soil-pile system, the empirical apparent fixity model underestimates the foundation stiffness remarkably, while the distributed spring model can give a relatively accurate prediction of the foundation stiffness. Moreover, the influence of the foundation modeling on the displacement and acceleration response is a little more significant than the internal force response. On the other hand, the apparent fixity model and distributed spring model miss the influence of soil condition on the displacement response which can be characterized in the FE model of the soil-pile system.

(b) An increase of the foundation stiffness with the increased pile diameter is observed for all three foundation modeling approaches, among which the apparent fixity model is more sensitive, while the other two almost show the same degree. Nevertheless, an increase in pile thickness results in a reduction of the displacement, among which the effect is more pronounced for the apparent fixity model but weakened for the other two foundation models

(c) Constant displacement response remains when the penetration is larger than 35.5 m after a reduction with the penetration depth ranging from 24 m to 35.5 m for the distributed spring model and the FE model of the soil-pile system. Furthermore, the FE model of soil-pile system is affected a little more notably than the distributed spring model.

(d) Considering the natural frequency, the apparent fixity model and FE model of the soil-pile model are recommended for the large foundation stiffness, whereas the distributed spring model takes the place of the apparent fixity model gradually with the decrease of the foundation stiffness. Nevertheless, as far as the tower top displacement is concerned, the distributed spring model is always superior to the apparent fixity model regardless of the foundation stiffness, with trivial discrepancies as compared with the benchmark FE model of the soil-pile system.

In the future, more engineering examples will be studied to validate the generality of the aforementioned conclusions and some other key issues, such as the soil plugging effect, need to be explored in depth. Furthermore, a complex soil model for cyclic loading needs to be incorporated into the soil-pile system to consider severe degradation in the upper soil layers subject to cyclic loading, which provides a more accurate prediction of the fatigue of wind turbines during the service life. In the meanwhile, analysis of the soil-pile system subject to the long-term cyclic wind and wave loading, which requires an excessive number of numerical iterations, will also be performed in the future study. On the other hand, the rotational sampling turbulence resulting from the rotation of the rotor blades plays an indispensable role in the fatigue damage of wind turbines, so the multiple peaks associated with the additional turbulence due to the rotation of the rotor blades and the wake effects of the upstream turbine will also be incorporated to the present model spectrum in our future study concerning the fatigue analysis of the downstream turbines in a wind farm. The present study serves as a preliminary exploration of the short-term dynamic performance of the wind turbine based on the FE model of the soil-pile system. The further extension to modeling complex loading conditions, especially long-term cyclic wind and wave loading, which contributes to the service life prediction of wind turbines and its structural optimization design, will be attached importance to the future line of research.

CRediT authorship contribution statement

Shanghui Yang: Methodology, Investigation, Software, Validation, Data curation, Writing – original draft, preparation. **Xiaowei Deng:** Conceptualization, Supervision, Writing – review & editing. **Jun Yang:** Conceptualization, Writing – review & editing.

Declaration of competing interest

The authors declare that they have no known competing financial interests or personal relationships that could have appeared to influence the work reported in this paper.

Acknowledgment

This work is generously supported by the Research Grants Council, ECS (RGC Ref No. 27209817) and CRF(C7038-20 GF), and National Natural Science Foundation of China, General Program (Project No. 51878586).

References

[1] D.Y. Leung, Y. Yang, Wind energy development and its environmental impact: a review, Renew. Sustain. Energy Rev. 16 (1) (2012) 1031–1039.
[2] S.-P. Breton, G. Moe, Status, plans and technologies for offshore wind turbines in Europe and North America, Renew. Energy 34 (3) (2009) 646–654.
[3] P. Schaumann, S. Lochte-Holtgreven, S. Steppeler, Special fatigue aspects in support structures of offshore wind turbines, Mater. Werkst. 42 (12) (2011) 1075–1081.
[4] D. Lombardi, Dynamics of Offshore Wind Turbines, University of Bristol UK, 2010.
[5] M. Achmus, Y.-S. Kuo, K. Abdel-Rahman, Behavior of monopile foundations under cyclic lateral load, Comput. Geotech. 36 (5) (2009) 725–735.
[6] J. van der Tempel, D.-P. Molenaar, Wind turbine structural dynamics–a review of the principles for modern power generation, onshore and offshore, Wind Eng. 26 (4) (2002) 211–222.
[7] S. Bisoi, S. Haldar, Dynamic analysis of offshore wind turbine in clay considering soil–monopile–tower interaction, Soil Dynam. Earthq. Eng. 63 (2014) 19–35.
[8] M. Zaaijer, Foundation modelling to assess dynamic behaviour of offshore wind turbines, Appl. Ocean Res. 28 (1) (2006) 45–57.
[9] P. Wang, M. Zhao, X. Du, J. Liu, C. Xu, Wind, wave and earthquake responses of offshore wind turbine on monopile foundation in clay, Soil Dynam. Earthq. Eng. 113 (2018) 47–57.
[10] S. Schafhirt, A.M. Page, G.R. Eiksund, M. Muskulus, Influence of Soil Parameters on the Fatigue Lifetime of Offshore Wind Turbines with Monopile Support Structure, 2016.
[11] N.D. Barltrop, A.J. Adams, Dynamics of Fixed Marine Structures, Butterworth-Heinemann, 2013.
[12] M.J. Kühn, Dynamics and Design Optimisation of Offshore Wind Energy Conversion Systems, DUWIND, Delft University Wind Energy Research Institute, 2001.
[13] M. Zaaijer, Foundation models for the dynamic response of offshore wind turbines, Proceedings of MAREC (2002) 1.
[14] D.N. Veritas, Design of Offshore Wind Turbine Structure, Offshore Standard DNV-OS-J101, 2004.
[15] A.P. Institute, Recommended Practice for Planning, Designing, and Constructing Fixed Offshore Platforms, American Petroleum Institute, 1989.
[16] D.A. Bouzid, S. Bhattacharya, L. Otsmane, Assessment of natural frequency of installed offshore wind turbines using nonlinear finite element model considering soil-monopile interaction, J. Rock Mechan. Geotechnic. Eng. 10 (2) (2018) 333–346.
[17] P. Doherty, K. Gavin, B. Casey, The geotechnical challenges facing the offshore wind sector, in: Geo-frontiers 2011: Advances in Geotechnical Engineering, 2011, pp. 162–171.
[18] I. Depina, T.M.H. Le, G. Eiksund, T. Benz, Behavior of cyclically loaded monopile foundations for offshore wind turbines in heterogeneous sands, Comput. Geotech. 65 (2015) 266–277.
[19] A. Haiderali, G. Madabhushi, Three-dimensional finite element modelling of monopiles for offshore wind turbines, in: Proceedings of the World Congress on Advances in Civil, environmental, and materials research, Seoul, 2012, pp. 3277–3295.
[20] S.S. Ahmed, B. Hawlader, Numerical analysis of large-diameter monopiles in dense sand supporting offshore wind turbines, Int. J. GeoMech. 16 (5) (2016), 04016018.
[21] H. Zuo, K. Bi, H. Hao, Dynamic analyses of operating offshore wind turbines including soil-structure interaction, Eng. Struct. 157 (2018) 42–62.
[22] H. Ma, J. Yang, L. Chen, Numerical analysis of the long-term performance of offshore wind turbines supported by monopiles, Ocean. Eng. 136 (2017) 94–105.
[23] E. Bush, L. Manuel, Foundation models for offshore wind turbines, in: 47th AIAA Aerospace Sciences Meeting Including the New Horizons Forum and Aerospace Exposition, 2009, p. 1037.
[24] S. Jung, S.-R. Kim, A. Patil, Effect of monopile foundation modeling on the structural response of a 5-MW offshore wind turbine tower, Ocean. Eng. 109 (2015) 479–488.
[25] K. Paik, R. Salgado, J. Lee, B. Kim, Behavior of open-and closed-ended piles driven into sands, J. Geotech. Geoenviron. Eng. 129 (4) (2003) 296–306.
[26] N. Strömblad, Modeling of Soil and Structure Interaction Subsea, 2014.
[27] C. Chen, P. Duffour, Modelling damping sources in monopile-supported offshore wind turbines, Wind Energy 21 (11) (2018) 1121–1140.
[28] N. Bazeos, G. Hatzigeorgiou, I. Hondros, H. Karamaneas, D. Karabalis, D. Beskos, Static, seismic and stability analyses of a prototype wind turbine steel tower, Eng. Struct. 24 (8) (2002) 1015–1025.
[29] L. Arany, S. Bhattacharya, J.H. Macdonald, S.J. Hogan, Closed form solution of

Eigen frequency of monopile supported offshore wind turbines in deeper waters incorporating stiffness of substructure and SSI, Soil Dynam. Earthq. Eng. 83 (2016) 18–32.
[30] M. Shinozuka, C.-M. Jan, Digital simulation of random processes and its applications, J. Sound Vib. 25 (1) (1972) 111–128.
[31] M. Shinozuka, G. Deodatis, Simulation of Stochastic Processes by Spectral Representation, 1991.
[32] J.C. Kaimal, J. Wyngaard, Y. Izumi, O. Coté, Spectral characteristics of surface-layer turbulence, Q. J. R. Meteorol. Soc. 98 (417) (1972) 563–589.
[33] P. Cuéllar, Pile Foundations for Offshore Wind Turbines: Numerical and Experimental Investigations on the Behaviour under Short-Term and Long-Term Cyclic Loading, 2011.
[34] F. Yu, J. Yang, Base capacity of open-ended steel pipe piles in sand, J. Geotech. Geoenviron. Eng. 138 (9) (2012) 1116–1128.
[35] F. Chen, Y. Lin, Y. Dong, D. Li, Numerical investigations of soil plugging effect inside large-diameter, open-ended wind turbine monopiles driven by vibratory hammers, Mar. Georesour. Geotechnol. 38 (1) (2020) 83–96.
[36] W. Wang, M. Yang, Review and discussion on key technologies in foundation design of offshore wind power, Shui Li Fa Dian Xue Bao 31 (6) (2012) 242–248.
[37] R.T. Klinkvort, O. Hededal, Lateral response of monopile supporting an offshore wind turbine, Proceed. Institut. Civil Eng.Geotechnic. Eng. 166 (2) (2013) 147–158.
[38] C. LeBlanc, G. Houlsby, B. Byrne, Response of stiff piles in sand to long-term cyclic lateral loading, Geotechnique 60 (2) (2010) 79–90.
[39] J.L. Briaud, T. Smith, B. Meyer, Using the pressuremeter curve to design laterally loaded piles, in: Offshore Technology Conference, 1983. Offshore Technology Conference.
[40] R. Dobry, E. Vicente, M. O'Rourke, M. Roesset, Horizontal stiffness and damping of single piles, J. Geotech. Geoenviron. Eng. 108 (GT3) (1982).
[41] H.G. Poulos, T. Hull, "The Role of Analytical Geomechanics in Foundation Engineering," Foundation Engineering: Current Principles and Practices, vol. 2, ASCE, Reston, 1989, pp. 1578–1606.